Applications of the Phase-Coded Generalized Hough Transform to Feature Detection, Analysis, and Segmentation of Digital Microstructures

Stephen R. Niezgoda[1] and Surya R. Kalidindi[1,2]

Abstract: The generalized Hough transform is a common technique for feature detection in image processing. In this paper, we develop a size invariant Hough framework for the detection of arbitrary shapes in three dimensional digital microstructure datasets. The Hough transform is efficiently implemented via kernel convolution with complex Hough filters, where shape is captured in the magnitude of the filter and scale in the complex phase. In this paper, we further generalize the concept of a Hough filter by encoding other parameters of interest (e.g. orientation of plate or fiber constituents) in the complex phase, broadening the applicability of Hough transform techniques. We demonstrate the application of these techniques to feature detection in micrographs (2-D) and three-dimensional (3-D) microstructure datasets, and explore their utility to the closely related applications of feature based image segmentation and calculation of 3-D microstructure metrics.

Keywords: microstructure, Hough transform, image processing, segmentation, feature detection

1   Introduction

The description of the internal structure (also referred to as the microstructure) of the material is at the core of all descriptions in the field of materials science and engineering. This internal structure is an exceptionally rich dataset that spans multiple hierarchical length scales from the macroscopic to atomistic. Recent advances in characterization techniques, such as 3-D atom probe (Blavette, Bostel, Sarrau, Deconihout and Menand 1993; Seidman 2007), x-ray micro-tomography (Flannery, Deckman, Roberge and D'amico 1987; Maire, Buffière, Salvo, Blandin, Ludwig and Létang 2001), 3-D x-ray diffraction microscopy (Schmidt, Nielsen,

---

[1] Department of Materials Science and Engineering, Drexel University, Philadelphia, 19104

[2] Department of Mechanical Engineering and Mechanics, Drexel University, Philadelphia, 19104. Corresponding author.

Gundlach, Margulies, Huang and Jensen 2004; Chapman, Barty, Marchesini, Noy, Hau-Riege, Cui, Howells, Rosen, He, Spence, Weierstall, Beetz, Jacobsen and Shapiro 2006), and automated serial sectioning, have made it possible to capture the three-dimensional details of microstructures at multiple length scales. The datasets generated from these techniques are often in the form of exceptionally large digital 3-D microstructure maps. For example, the high-resolution tomography capabilities at the European Synchrotron Radiation Facility can capture a field of view of 2048 x 2048 pixels at a $0.28\mu m$ pixel size and exceeding 8GB in the size of the dataset, with the reconstructed 3-D voxel dataset exceeding 8×10^9 voxels (Betz, Wegst, Weide, Heethoff, Helfen, Lee and Cloetens 2007). Visualization and analysis of such large datasets is a non-trivial problem. Depending on the scale of the microstructural features of interest, a reconstructed 3-D volume may contain upwards of 100,000 examples. Manually scanning such a dataset for microstructural features or defects (e.g. cracks, pores) is time consuming, and often impractical. In order to rigorously study these datasets, an automated methodology to locate features of interest is critically needed.

In this paper, we explore the application of a phase-coded generalized Hough transform to the problem of automated microstructure feature detection. We also explore the closely related applications of feature-based image segmentation and calculation of 3-D microstructure metrics. The generalized Hough transform is a name given to a class of algorithms for the detection of imperfect instances of a target object in an image or volume. The original Hough transform was conceived as a method for extracting lines and simple curves from images (Hough 1962; Duda and Hart 1972), and is probably best known to materials scientists in its application to the automated indexing of electron backscatter diffraction (EBSD) for orientation imaging microscopy (OIM) (Adams, Wright and Kunze 1993; Schwartz, Kumar and Adams 2000). The basic Hough transform has been generalized for the detection of arbitrary shapes (Ballard 1981) and has been efficiently implemented via kernel convolution (Kierkegaard 1992). Atherton and Kerbyson developed a complex Hough filter for size invariant circle detection (Kerbyson and Atherton 1995; Atherton and Kerbyson 1999). Here we further extend the general framework of Atherton and Kerbyson to the detection of 3-D arbitrary shapes in microstructure datasets and extend the complex Hough filter to size invariant shape detection and orientation invariant line detection. We will then demonstrate the utility of this framework in three specific examples: 1) The detection of grains with a specified morphology in a polycrystalline material, 2) The rapid calculation of a common statistical microstructure metric referred to as the lineal path function (Lu and Torquato 1992), and 3) The segmentation of an alpha/beta titanium colony microstructure into individual colonies.

2   Phase-Coded Generalized Hough Filters

The Hough transform was originally developed for the machine analysis of trajectories of charged sub-atomic particles in a bubble chamber (Hough 1962). The Hough transform is an elegant mapping of each pixel in a binary image to a sinusoidal curve in an accumulator or voting space, so that curves corresponding to collinear pixels intersect in the voting space. We quickly review the basic Hough transform since the key concepts are carried through to the more complex Hough filters developed in this work.

Any line in a 2-D plane can be parameterized by the length of the perpendicular from the line to the origin, r, and by the angle of this perpendicular, θ, as $r = x\cos\theta + y\sin\theta$. Thus every possible line in the plane can be uniquely mapped to a point in the parameter space as the ordered pair (r, θ). Each pixel in an image is mapped to a curve in the parameter space through the realization that all possible lines passing through the point (x_0, y_0) have the form $r(\theta) = x_0\cos\theta + y_0\sin\theta$, which is a sinusoid through the parameter space. If the curves from two pixels in the image are plotted in the parameter space, the intersecting point corresponds to the line connecting those points in the image. Lines in the binary image can then be easily found by mapping all of the pixels from the binary image into the parameter space and counting the number of intersections at each point. The points where numerous curves intersect correspond to line segments in the image. Thus the parameter space is referred to as the voting or accumulator space, as each intersection is considered a vote for a possible line in the image. Longer or more perfect line segments will receive more votes as more curves in the accumulator space will intersect.

The circle Hough transform can be used to detect circles in an image in a very similar manner. The standard equation of a circle in a 2-D plane, $(x - a)^2 + (y - b)^2 = r^2$ parameterizes the circle by the ordered triplet (a, b, r). Each pixel in the image can be mapped to a right circular cone in the parameter space (see Figure 1 and description below). The cones from all of the edge points on a circle will intersect at a single point in the space (Duda and Hart 1972). In parallel with the line case larger circles or more perfect circles will receive more votes. This simple observation will motivate the introduction of a corrective normalization in later examples. In general such a mapping can be constructed for any shape described by a set of parametric equations, where the dimensionality of the accumulator space is determined by the number of parameters.

The conventional Hough transforms described above can be formulated as a series of convolutions with a series of appropriately defined Hough transform filters. For example, consider a binary digital image where each pixel can either take the values
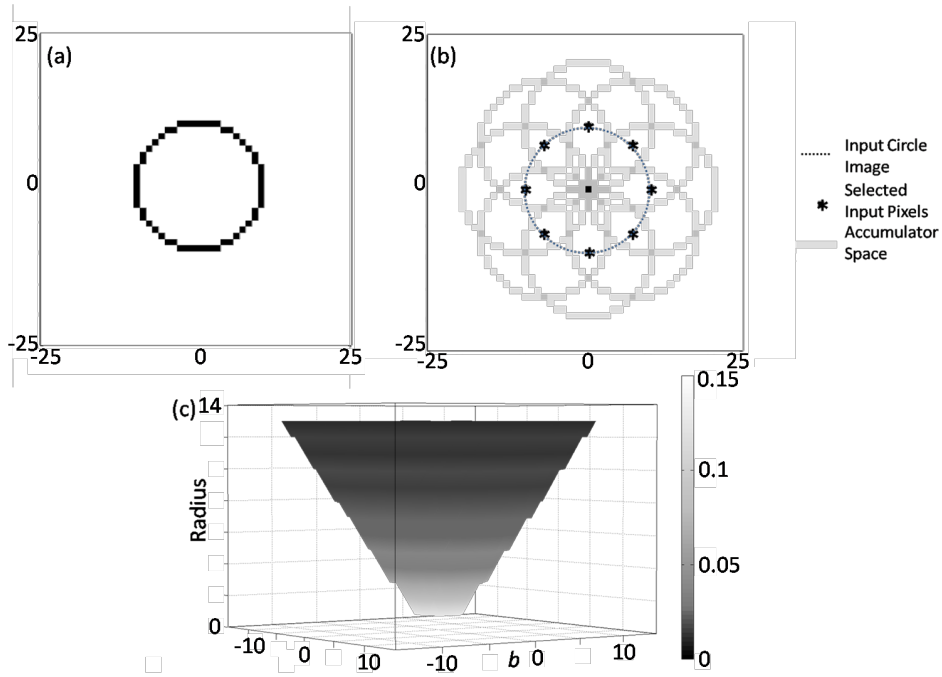
Figure 1: (a) Hough filter for a circle of radius 10 as defined by Eq. (1). (b) The contribution of selected pixels in the accumulator space of the convolution of a circle (schematically shown by the dotted line) with the filter shown in (a). The effect of the convolution operation is to "draw" in a circle of radius 10 at each pixel. These circles intersect at the point $(a = 0, b = 0)$ in the accumulator space. High intensity pixels in the accumulator space indicate likely centers of circles in the image space. (c) The (a, b, r) accumulator space resulting from the convolution of a single pixel located at the origin with a successive series of filters from $r^* = 1$ to $r^* = 13$. The effect of the circle Hough transform is to map each pixel in the image to a right circular cone in the full accumulator space.

0 or 1, in which we wish to detect a circle of radius r^* pixels. The corresponding Hough filter will be of size $(2r^* + 1, 2r^* + 1)$ where the rows of the filter are indexed $m = [-r^*, -r^* + 1, \ldots, 0, \ldots, r^* - 1, r^*]$, and the columns are similarly indexed by n. The filter can then be defined as

$$\mathscr{O}_{mn} = \begin{cases} \frac{1}{2\pi r^*} & \text{iff } (r^* - 0.5)^2 < m^2 + n^2 < (r^* + 0.5)^2 \\ 0 & \text{otherwise} \end{cases} \qquad (1)$$

which is simply a circle of radius r^* normalized so that its power is 1. Convolution

with the filter maps a pixel located at position (a_0, b_0) in the image to a circle with equation $(x - a_0)^2 + (y - b_0)^2 = (r^*)^2$ in the accumulator space, with an intensity of $\frac{1}{2\pi r^*}$. If the image contains a perfect circle of radius r^* centered at position (a_0, b_0), the set of edge pixels will each be mapped to a circle of radius r^* in the accumulator space that all share the common point (a_0, b_0). Each circle contributes $\frac{1}{2\pi r^*}$ to the intensity at the intersection point in the accumulator space (see Figure 1). The purpose of normalizing the power of the filter by $\frac{1}{2\pi r^*}$ is so that the cumulative contribution of all the edge points of a perfect circle in the image is unity. Thus the problem of detecting circles of radius r^* in the image is reduced to identifying pixels in the accumulator space with intensity close to 1. By "stacking" the results of successive convolutions with filters ranging from $r^* = r^{\min}$ to $r^* = r^{\max}$ the desired portion of the accumulator space, (a, b, r), can be explored. The mapping of a single pixel to a right circular cone in the accumulator space is shown in Figure 1. Hough filters offer significant computational advantages as the convolution operations can be efficiently computed via fast Fourier transform (FFT) methods (Briggs and Henson 1995). The primary advantage of filter based techniques is the elimination of the need for an analytic parametric description of the shape being detected; with an appropriately defined filter the above approach is applicable to the detection of arbitrary shapes (Ballard 1981; Samal and Edwards 1997).

The drawback of the above approach is that a different filter is needed for each r^*, i.e. the technique is not scale invariant. Atherton and Kerbyson proposed a complex Hough filter for size invariant circle detection in 2-D binary images (Kerbyson and Atherton 1995; Atherton and Kerbyson 1999). Here, we present a framework based on the Atherton and Kerbyson filters, with an added normalization to improve accuracy when searching over a wide range of sizes and extended to the detection of arbitrary shapes in 3-D microstructure datasets. The general principal behind this approach is to reduce the dimensionality of the accumulator space by encoding scale information in the complex phase of the filter. For circles, the filter is a annulus where the phase varies linearly from $r^{min} \rightarrow r^{max}$, defined by

$$\mathscr{O}_{mn} = \begin{cases} \frac{1}{2\pi\sqrt{m^2+n^2}} e^{2\pi i \phi_{mn}} & \text{iff } (r^{min})^2 \leq m^2 + n^2 \leq (r^{max})^2 \\ 0 & \text{otherwise} \end{cases}$$

$$\phi_{mn} = \frac{\sqrt{m^2+n^2} - r^{min}}{r^{max} - r^{min}}$$

(2)

An example filter is shown in Figure 2.

When convoluted with an image containing a circle of radius r^*, the contribution from each edge pixel on the circle will interfere constructively for the phase corresponding to r^* and destructively for all other phases. Thus the intensity of the
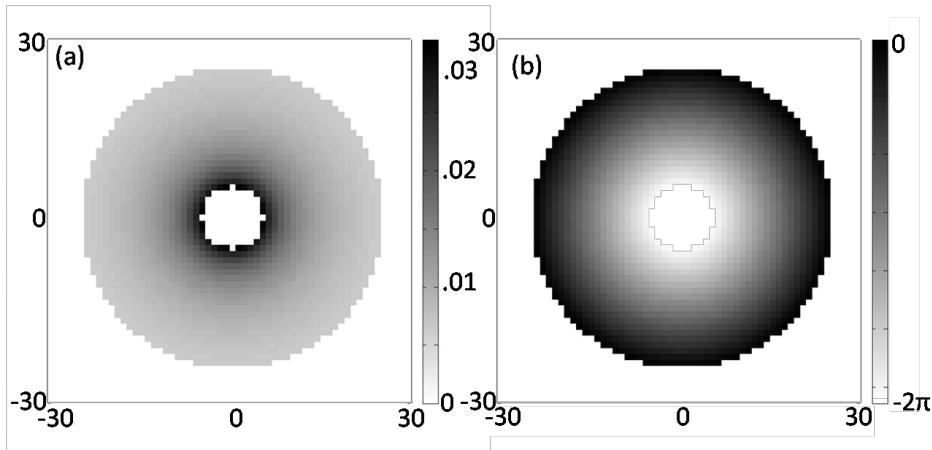
Figure 2: Complex phase coded Hough filter defined by Eq. (2) with $r^{min} = 5$ and $r^{max} = 25$. The complex magnitude as a function of radius is shown in (a) and the phase angle is shown in (b).

accumulator space gives the likelihood of finding a circle centered at that location in the image, and the phase gives the radius of the circle. The normalization by $\frac{1}{2\pi\sqrt{m^2+n^2}}$ in Eq. (2) is designed so that all circles contribute equal intensity to the accumulator space regardless of size. To the best knowledge of the authors, this is a novel contribution from this work. Without such normalization, the peaks in accumulator space from different sized circles are proportionate to their circumference. For ideal images of perfect circles without any signal noise, this difference in peak height is not of great consequence. However, for noisy images and images with imperfect features (such as characterized micrographs), this normalization greatly improves the ability to accurately detect small circles, especially when $r^{max} \gg r^{min}$. Additionally, normalizing the contribution of a perfect circle to unity, allows the intensity in the accumulator to be thought of as a probability on the likelihood of a circle being centered at that point. For example, an accumulator point with intensity 0.9 indicates that 90% of the pixels are consistent with a perfect circle. With the added normalization, this technique is quite robust, even for noisy images, when detecting circles with a wide distribution of radii. The application of our normalized phase coded filter to circle detection in a perfect and noisy image is detailed in Figure 3.

The circular filters described above for 2-D images are an important theoretical and intellectual exercise. However, these filters need to be extended to arbitrary shapes in 3-D in order to be of significant practical use for microstructure analysis.
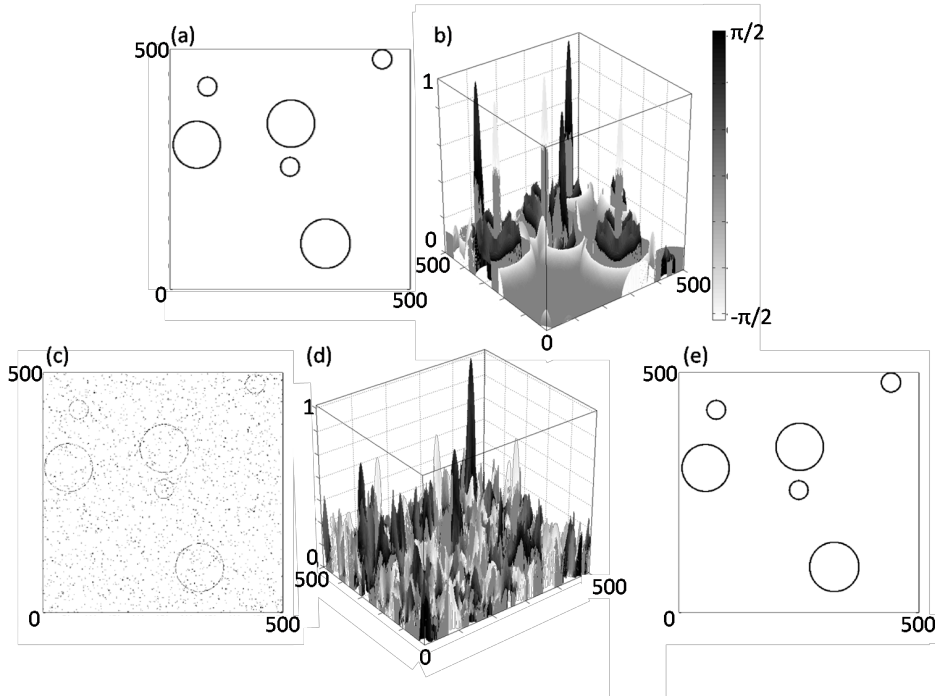
Figure 3: (a) Ideal digital image containing circles of radius 20 and 50 pixels. (b) Accumulator space plotted as surface resulting from convolution of image (a) with filter defined by Eq. (2) where $r^{min} = 10$ and $r^{max} = 60$. Height of the peak indicates complex magnitude and coloration gives complex phase. There are indeed six main peaks in this plot, and their phase correctly reflected the corresponding circle radii. (c) Digital image containing imperfect circles and added uniformly distributed noise at a volume fraction of 0.15. (d) Accumulator space for image (c). The noise adds additional peaks to the space and the peaks corresponding to circles have been diminished relative to the ideal case. (e) Reconstructed image from the accumulator space, by thresholding the accumulator space at 0.5 to separate the desired peaks from the spurious ones due to the noise in the image.

Note that the extension of Eq. (2) from circles to spheres is trivial, the form remains exactly the same and the appropriate normalization becomes surface area rather than circumference. Consider an arbitrary 3-D solid shape (such as a grain in a polycrystalline material) denoted ω and described by the indicator function

(Torquato 2002):

$$\mathscr{I}_{mnp} = \begin{cases} 1 & \text{if pixel } m,n,p \text{ is interior to } \omega \\ 0 & \text{if pixel } m,n,p \text{ is exterior to } \omega \end{cases} \tag{3}$$

The surface of ω can then be expressed as (Torquato 2002)

$$\mathscr{M}_{mnp} = |\nabla \mathscr{I}_{mnp}| \tag{4}$$

which is nonzero only at the surface pixels. Additionally, let $A = \sum_{m,n,p} \mathscr{M}_{mnp}$ indicate the number of surface pixels. A simple Hough filter to find exact instances of ω could be defined as

$$\mathscr{O}_{mnp} = \frac{1}{A} \mathscr{M}_{mnp} \tag{5}$$

To develop a complex filter for size invariant detection we introduce the notation $\mathscr{M}_{mnp}^s$ where the index indicates a scaling factor, i.e. $\mathscr{M}_{mnp}^2$ are the surface pixels when the size of is scaled by 2. Similarly, let $A_s = \sum_{m,n,p} \mathscr{M}_{mnp}^s \approx A_1 s^2$ represent the appropriate scaling for surface area. A general size invariant Hough filter can thus be defined as

$$\mathscr{O}_{mnp} = \int_{s^{min}}^{s^{max}} \frac{1}{A_s} e^{2\pi i \phi^s} \mathscr{M}_{mnp}^s ds$$
$$\phi^s = \frac{s - s^{min}}{s^{max} - s^{min}} \tag{6}$$

An example of a filter modeled on a single grain from a polycrystalline dataset is shown in Figure 4.

In effect, a complex filter allows us to reduce the dimensionality of the accumulator space by encoding one parameter in the phase. In the examples described in Eqs. (2) and (6), the phase angle represented scale. For other feature identification applications, it might be more advantageous to encode a different microstructure feature as the phase. As an example, consider the problem of rapidly identifying the orientation of fibers in a 2-D micrograph from a fiber-reinforced composite. In this case, a convolution with a simple filter of the form (in polar coordinates)

$$\mathscr{O}_{r\theta} = \begin{cases} \frac{1}{r^*} e^{2\pi i \frac{\theta}{\pi}} & \text{if } r \leq r^* \\ 0 & \text{otherwise} \end{cases} \tag{7}$$

where is approximately equal to the average fiber length, will indentify the orientation associated with each fiber. This example and related applications will be
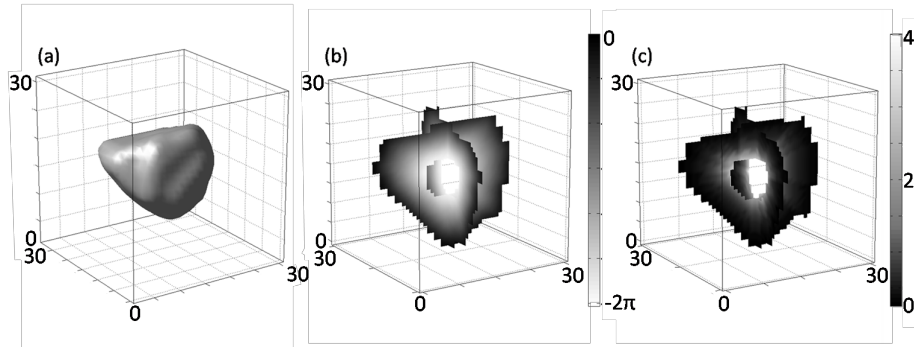
Figure 4: (a) A single grain extracted from a digital polycrystalline microstructure that served as a template for the filter shown in (b) and (c). (b,c) Intersecting orthogonal slices through the center of the filter corresponding to the image in (a) obtained by using Eq. (6). (b) shows the complex phase of the filter, and (c) shows the magnitude. Only pixels that take non-zero values are visible.

explored in more detail in the Image Segmentation section below. In the image processing literature, the term Hough filters is only used for feature extraction applications, and would not necessarily cover Eq. (7). However, for our purposes, the implementation and interpretation are so similar that we will refer to them as generalized Hough filters.

3   Feature Extraction in Digital Microstructures

In order to validate the framework presented earlier, we will apply the Hough filters defined by Eq. (6) to extract grains of a prescribed morphology from a digitally created polycrystalline microstructure (Brahme, Alvi, Saylor, Fridy and Rollett 2006). The microstructure is 100x100x100 pixels in size and contains 997 unique grains (see Figure 5). The Hough filter techniques described above rely on the mapping of edge pixels into the accumulator space. Thus the first step in extracting grains based on morphology is to convert the full dataset into a grain boundary network. This was accomplished using a simple Canny edge detection algorithm on the individual 2D slices (Canny 1986), and the results are shown in Figure 5. For complex datasets, more robust edge segmentation algorithms would be required. The dataset was then searched for grains of 2 specific morphologies: 1) spherical grains and 2) grains similar in shape and scale to a specified target grain. The dataset shown in Figure 5 is perfectly periodic, thus it was natural to include edge grains that intersect the bounding box. For aperiodic digitally created or characterized datasets the decision to include the edge grains would have to be informed by both the applica-

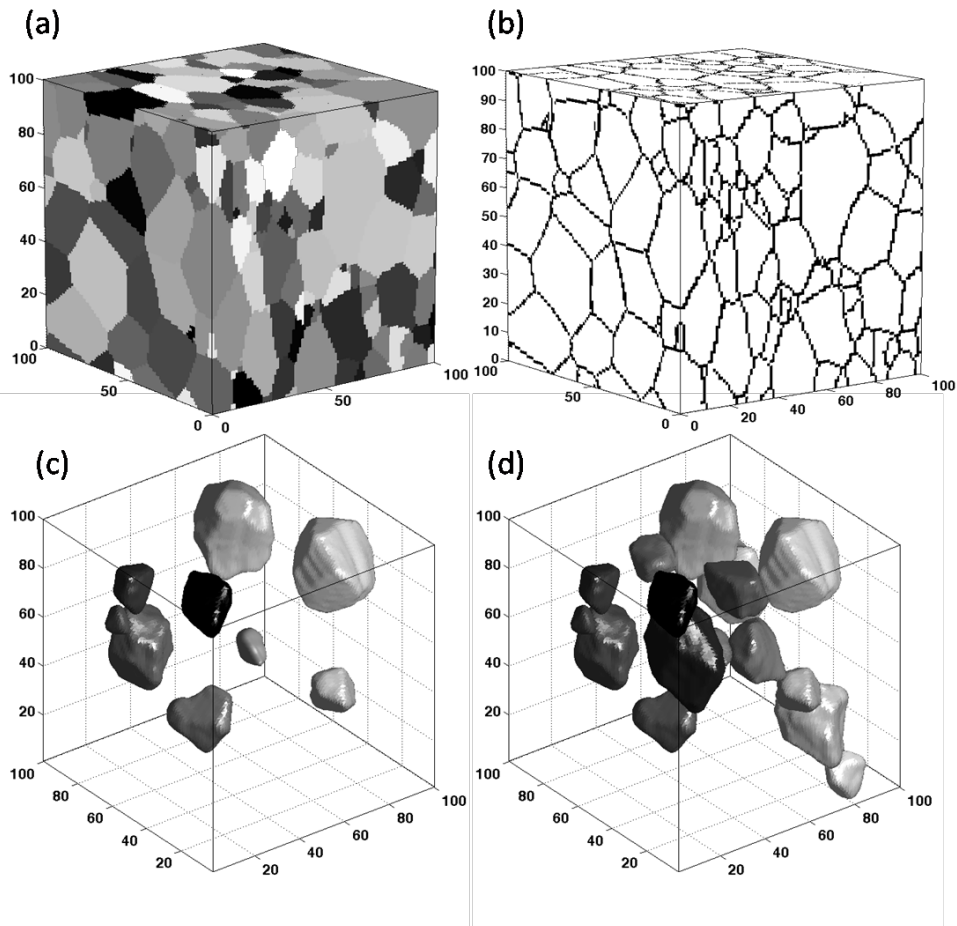tion and the shapes being detected.

Figure 5: (a) Digitally created polycrystalline dataset 100x100x100 pixels in size. The dataset contains 997 unique grains. (b) Grain boundary network created from edge detection on the entire dataset. The Hough filters act on the edge pixels and accurate edge detection is critical to shape detection. (c) Equi-axed grains extracted from the dataset in (a) at an accumulator threshold of 0.28 (97% of the maximum intensity), the radius range of the filter was 5 to 20 pixels. (d) By lowering the threshold to 0.26 (90% of the maximum intensity) more grains are detected, however while still equi-axed, the selected grains have a larger deviation from spherocity.

The results of the spherical grain detection are shown in Figure 5. A spherical filter was defined based on Eq. (6), where $\mathcal{M}_{mnp}$ was a spherical shell of radius 10, $s^{min} = 0.5$, and $s^{max} = 2$. Thus, the working range of the filter was radii between 5 and 20 pixels. After convolution, the maximum magnitude of the accumulator space was 0.29, indicating that for the most spherical grain, only about 30% of the pixels coincided with a perfect sphere. In this case the relatively low intensities in the accumulator space are not surprising; the fact that grains are space filling structures precludes the existence of perfectly spherical grains. Here, the higher intensity regions in the accumulator space after convolution with a spherical filter correspond to the locations of the most equi-axed grains in the microstructure. The results are shown for two threshold values in the accumulator space, 0.28 and 0.26 (97% and 90% of the max value respectively). At the 0.28 level, the grains that are extracted appear to deviate substantially from spherical. On closer inspection it is seen that these grains are largely equi-axed with local deviations; when viewed from another angle they appear nearly spherical. At the 0.26 level, the deviation from spherocity is more evident but the grains are clearly still equi-axed.

When applied to detecting near instances of natural shapes common in the dataset, the generalized Hough filters are extremely robust. A Hough filter was created based on an archetype grain from the dataset and was used to extract grains of similar shape and scale. A pancaked archetype grain was selected to differentiate the results from the spherical filter case, and a narrow scale range of $s^{min} = 0.8$ to $s^{max} = 1.2$ was used. The archetype grain and the nearest other grains are shown in Figure 6. Since the filter was constructed from an actual grain from the sample, the intensity of the accumulator space ranges from 0 to 1, with accumulator intensity 1 indicating the center of mass from the archetype grain. After the grain that served as a template, the next highest peak in the accumulator space has an intensity of 0.4. Thresholding the accumulator space at 0.30 left only the peaks corresponding to the archetype grain and the 5 closest grains.

The low values of peaks in the accumulator space for both the spherical and naturally shaped filter highlight the need for proper normalization of the phase coded filter. In microstructural feature detection we are naturally seeking imperfect instances of the object; no two grains are the same morphology.

4   Lineal Path Function and Related Functions

The lineal path function is an important statistical descriptor of the microstructure which is often used in reconstructions of 3-D microstructures from 2-D sections (Yeong and Torquato 1998; Manwart, Torquato and Hilfer 2000; Zeman and Sejnoha 2007). Additionally, the lineal path function contains linear free path information and has been used to model Knudsen diffusion and radiative transport in
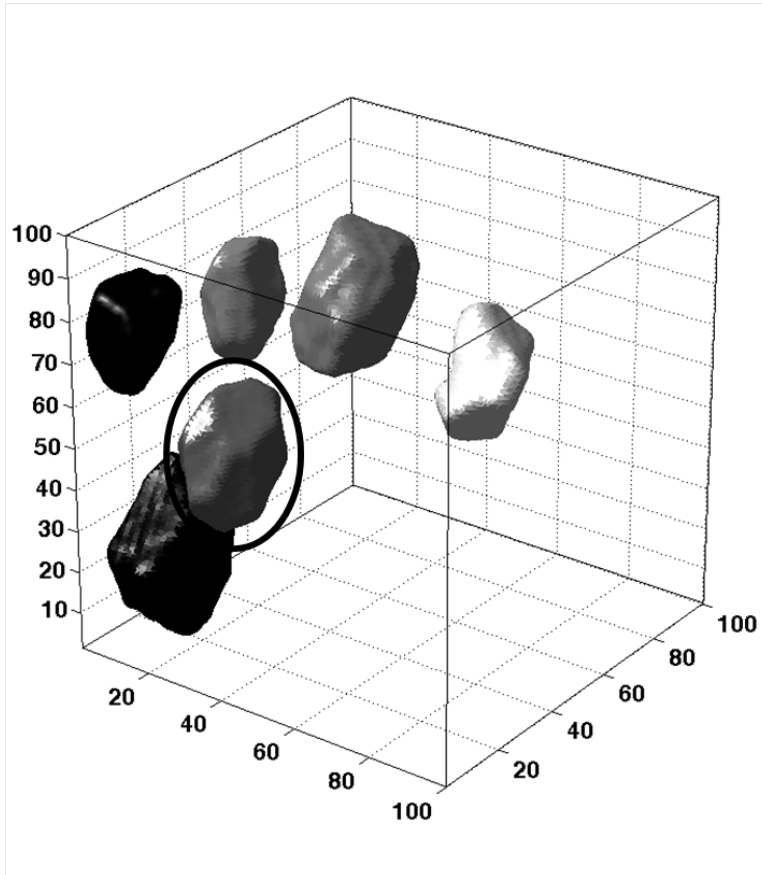
Figure 6: Grains from the dataset shown in Figure 5 that come closest to matching the circled archetype grain in shape and scale. The edge pixels of the circled grain were used to construct a Hough filter using Eq. (6). Thresholding the accumulator space at 30% returned the archetype grain and 5 most similar grains.

porous materials (Torquato 2002). The lineal path function, i, is defined as the probability that a line segment of length z lies entirely in phase i when thrown randomly into the microstructure. The lineal path function is commonly calculated by sampling, and accurate measurement requires throwing a very large number of line segments into the microstructure (Torquato 2002; Singh, Gokhale, Lieberman and Tamirisakandala 2008). Most applications of the lineal path function are limited to isotropic structures and the function is assumed to be independent of the orientation of line segment. For broad applicability to anisotropic structures, the lineal path function must be calculated as function of the length of line segment i and also

its orientation, i.e. $L^i(\mathbf{z})$, where $\mathbf{z}$ is a 2-D or 3-D vector. This angularly resolved lineal path function is rarely calculated, or is only calculated at a handful of angles, due to the tedious nature of the required sampling over the space of length and orientations (Singh, Gokhale, Lieberman and Tamirisakandala 2008).

Calculation of the angularly resolved lineal path function can be efficiently achieved using generalized Hough filter approaches described earlier. For example, the filter to calculate $L^i(z = z^*, \theta = \theta^*)$ in a 2-D microstructure can be expressed as

$$
\mathscr{O}_{r\theta} = \begin{cases} \frac{1}{r^*} & \text{if } r \leq r^* \text{ and } \theta = \theta^* \\ 0 & \text{otherwise} \end{cases} \tag{8}
$$

Convolution of a properly segmented microstructure image with the above filter will map a value of 1 everywhere the vector $\mathbf{z}$ will fit in the image. $L^i(z = z^*, \theta = \theta^*)$ is simply calculated as the fraction of accumulator space pixels with value 1. In a sense, the Hough filter can be thought of as sampling every possible placement of vector $\mathbf{z}$, defined by the ordered pair (z, θ), simultaneously. Thus the entire lineal path function $L^i(\mathbf{z})$ can be calculated by convolution with a series of Hough filters where the length and orientation of the vector $\mathbf{z}$ are systematically varied. An example calculation of the lineal path function for a 2-phase microstructure is shown in Figure 7. When calculating statistical measures in this way it is important to consider bias due to boundary effects due to the convolution operation by either padding the image or discounting the contribution of points near the boundary (Briggs and Henson 1995)(Gokhale, Lieberman and Tamirisakandala 2008).

The use of Hough filters allows further generalization of the lineal path function. Rather than simply calculating the probability of an oriented line segment falling completely in a selected phase, we can calculate the probability associated with other shapes. For example in 3-D percolating microstructures, the flux through a region is strongly dependent on the cross-sectional area of the connected paths. In this case, a better statistical measure might be the probability that sphere of radius r or a cylinder of radius r, length z and a orientation (θ, ϕ) falls within a selected phase. As a simple example, determination of the radial path function $R^i(r)$ (probability of a sphere of radius r lies completely in phase i when thrown randomly into the microstructure) for a porous solid is shown in Figure 7.

5 Application to Image Segmentation

Segmentation of an experimentally characterized microstructure, especially in 3-D, based on microstructural features is a difficult task without a general solution. The approach taken is highly subjective to both the characterization technique and microstructure (for interesting examples, see (Chawla, Ganesh and Wunsch 2004;
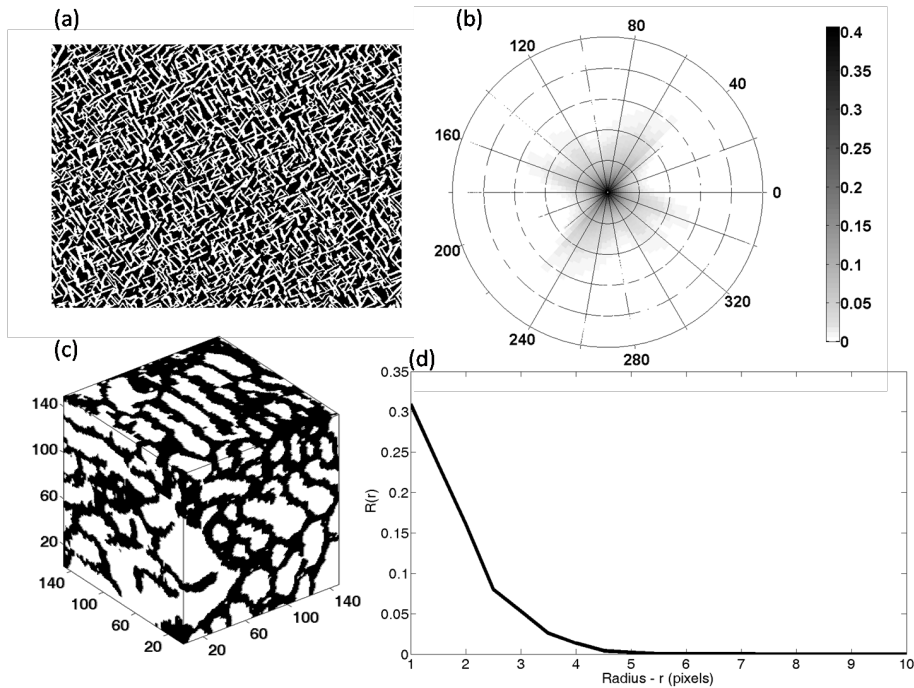
Figure 7: (a) Digital image of a two phase microstructure showing a clear anisotropy in platelet orientation. Microstructure image is 2904x3864 pixels. (b) Angularly resolved lineal path function $L^i(z)$ calculated by convolution of the microstructure shown in (a) with a series of filters defined by Eq. (8). Each meridian represents the lineal path function for line segments of a given angular orientation. Each radius represent a given line segment length. The radial range is from 0-240 pixels with a gridline every 56 pixels. Notice that anisotropy of the microstructure is clearly captured in the lineal path function. (c) Digitally created 3-D porous solid. The white phase indicates pore and the solid is black. (d) Radial path function calculated from (c). The radial path function gives the probability that a sphere of radius r lands completely in the pore space, when thrown randomly into the microstructure.

Petushi, Katsinis, Coward, Garcia and Tozeren 2004; Stutzman 2004; Uchic, Groeber, Dimiduk and Simmons 2006; Simmons, Bartha, De Graef and Comer 2008)). Often, the problem of image segmentation can be simplified by the application of a suitably defined phase-coded Hough filter. As a simple example, consider the back-scattered electron (BSE) image of an alpha/beta titanium colony microstructure shown in Figure 9, obtained in a scanning electron microscope (SEM). In char-
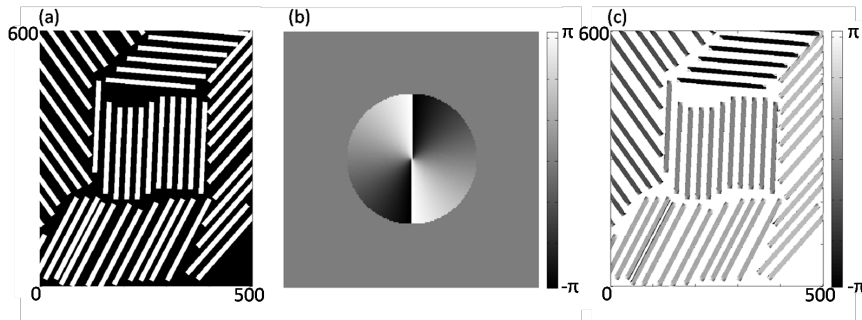
Figure 8: (a) Idealized lath or plate microstructure to serve as a demonstration for orientation resolution by the generalized Hough filter. (b) Complex phase of an orientation resolving Hough filter built using Eq. (7) with $r^* = 50$; the polar angle is encoded as the complex phase. The magnitude of the filter is 1 for $r \leq 50$ and zero otherwise. (c) Result of convolution of the image (a) and the filter (b). The image shows the complex phase of pixels corresponding to the laths (white) in (a). For clarity, the complex phase of the other pixels (black) are not shown. The orientation of the lath can then be read directly from the phase information.

acterizing such a microstructure, one often desires to extract statistics from individual colonies such as the mean lath separation or the volume fraction of alpha (Tiley, Searles, Lee, Kar, Banerjee, Russ and Fraser 2004; Collins, Welk, Searles, Tiley, Russ and Fraser 2009). An automated method of segmenting the microstructure into colonies would be extremely beneficial.

The problem of colony segmentation can be effectively addressed through the application of a generalized Hough filter to resolve the lath orientation. For clarity we will demonstrate the approach on an idealized plate or lath microstructure (see Figure 8), and subsequently show the results for the experimentally acquired micrograph shown in Figure 9. A line orientation encoding Hough filter was created using Eq. (7) with $r^* = 50$ pixels. The magnitude of the filter is 1 inside the circle and zero outside, and the complex phase is shown in Figure 8. When convolved with the microstructure image the phase corresponding to the orientation constructively interferes in the accumulator space. The complex phase of each line can then be mapped back to a physical orientation angle. The image can be segmented in the accumulator space by simply isolating regions of similar complex phase. Notice that the areas near the end of the laths or where two laths are near each other exhibit slight variance in phase relative to the center, which is largely due to the edge effects from convolution. At points near the edge of features, the filter has less complete destructive interference of the other phases. For the same reason,
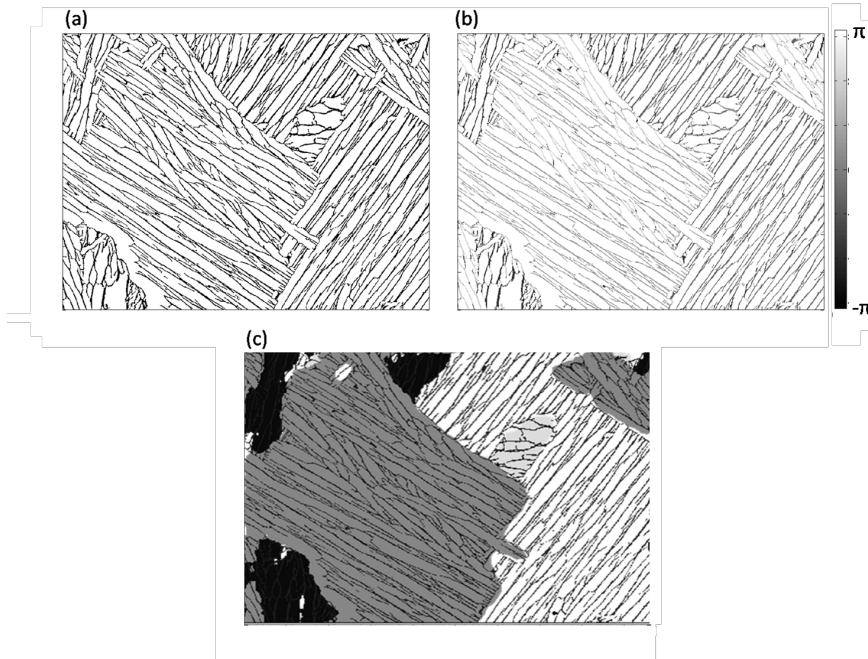
Figure 9: (a) A BSE SEM image of an alpha/beta colony microstructure in titanium. The microstructure is to be segmented into colonies based on the local lath orientation. (b) Complex phase of the accumulator space resulting from the convolution of the image with an orientation resolving Hough filter. (c) The micrograph is segmented into colonies by grouping regions of similar orientation (similar complex phase) in the accumulator space.

the intensity of the accumulator space will also be lower at these points relative to the center of the laths. The intensity in the accumulator space can then serve as a metric on the quality of the data at each pixel. If the phase information is to be used for a quantitative analysis, such as on fiber orientation distribution, low quality pixels can be eliminated and replaced by flood filling (or other suitable technique) from high quality data points. Figure 9 shows results of the same procedure on an experimentally obtained BSE SEM micrograph of alpha/beta titanium colony.

6   Summary

In this paper we developed and validated a framework based on generalized Hough transform filters for successful automated extraction of microstructural features and related applications. Specifically, we developed size invariant filters for feature de-

tection in 3-D by encoding scale information in the complex phase of the Hough filters. The filters were formulated for the detection of arbitrary shapes eliminating the need for an analytical parameterization. The concept of a Hough filter was further generalized by considering complex filters that encode other parameters such as line orientation, thus broadening the utility of the generalized Hough transform to a host of other microstructure analysis applications. Several examples were presented on feature extraction in polycrystalline 3-D digital microstructure datasets as would be obtained from serial sectioning. The application of generalized Hough filters to the rapid calculation of the angularly resolved lineal path function and other related statistical metrics was demonstrated in 2-D. Additionally, we demonstrated the utility of orientation coded Hough filters to successfully address automated, feature based, microstructure segmentation.

References

Adams, B., S. Wright, K. Kunze (1993): Orientation imaging: The emergence of a new microscopy. *Metallurgical and Materials Transactions A* **24**(4): 819-831.

Atherton, T. J., D. J. Kerbyson (1999): Size invariant circle detection. *Image and Vision Computing* **17**(11): 795-803.

Ballard, D. H. (1981): Generalizing the Hough transform to detect arbitrary shapes. *Pattern Recognition* **13**(2): 111-122.

Betz, O., U. Wegst, D. Weide, M. Heethoff, L. Helfen, W.-K. Lee, P. Cloetens (2007): Imaging applications of synchrotron X-ray phase-contrast microtomography in biological morphology and biomaterials science. I. General aspects of the technique and its advantages in the analysis of millimetre-sized arthropod structure. *Journal of Microscopy* **227**(1): 51-71.

Blavette, D., A. Bostel, J. M. Sarrau, B. Deconihout, A. Menand (1993): An atom probe for three-dimensional tomography. *Nature* **363**(6428): 432-435.

Brahme, A., M. H. Alvi, D. Saylor, J. Fridy, A. D. Rollett (2006): 3D reconstruction of microstructure in a commercial purity aluminum. *Scripta Materialia* **55**(1): 75-80.

Briggs, W. L., V. E. Henson (1995): *The DFT : an owner's manual for the discrete*

Fourier transform. Philadelphia, Society for Industrial and Applied Mathematics.

Canny, J. (1986): A Computational Approach to Edge Detection. *Pattern Analysis and Machine Intelligence, IEEE Transactions on* **PAMI-8**(6): 679-698.

Chapman, H. N., A. Barty, S. Marchesini, A. Noy, S. P. Hau-Riege, C. Cui, M. R. Howells, R. Rosen, H. He, J. C. H. Spence, U. Weierstall, T. Beetz, C. Jacobsen, D. Shapiro (2006): High-resolution ab initio three-dimensional x-ray diffraction microscopy. *J. Opt. Soc. Am. A* **23**(5): 1179-1200.

Chawla, N., V. V. Ganesh, B. Wunsch (2004): Three-dimensional (3D) microstructure visualization and finite element modeling of the mechanical behavior of SiC particle reinforced aluminum composites. *Scripta Materialia* **51**(2): 161-165.

Collins, P. C., B. Welk, T. Searles, J. Tiley, J. C. Russ, H. L. Fraser (2009): Development of methods for the quantification of microstructural features in [alpha] + [beta]-processed [alpha]/[beta] titanium alloys. *Materials Science and Engineering: A* **508**(1-2): 174-182.

Duda, R. O., P. E. Hart (1972): Use of the Hough transformation to detect lines and curves in pictures. *Commun. ACM* **15**(1): 11-15.

Flannery, B. P., H. W. Deckman, W. G. Roberge, K. L. D'amico (1987): Three-Dimensional X-ray Microtomography. *Science* **237**(4821): 1439-1444.

Hough, P. V. C. (1962): *Method and means for recognizing complex patterns. U.S. Patent No. 3069654.*

Kerbyson, D. J., T. J. Atherton (1995): Circle detection using Hough transform filters. Image Processing and its Applications, 1995., Fifth International Conference on.

Kierkegaard, P. (1992): A method for detection of circular arcs based on the Hough transform. *Machine Vision and Applications* **5**(4): 249-263.

Lu, B., S. Torquato (1992): Lineal-path function for random heterogeneous materials. *Physical Review A* **45**(2): 922.

Maire, E., J. Y. Buffière, L. Salvo, J. J. Blandin, W. Ludwig and J. M. Létang (2001): On the Application of X-ray Microtomography in the Field of Materials Science. *Advanced Engineering Materials* **3**(8): 539-546.

Manwart, C., S. Torquato, R. Hilfer (2000): Stochastic reconstruction of sandstones. *Physical Review E* **62**(1): 893.

Petushi, S., C. Katsinis, C. Coward, F. Garcia, A. Tozeren (2004): Automated identification of microstructures on histology slides. Biomedical Imaging: Nano to Macro, 2004. IEEE International Symposium on.

Samal, A., J. Edwards (1997): Generalized Hough transform for natural shapes.

Pattern Recognition Letters **18**(5): 473-480.

Schmidt, S., S. F. Nielsen, C. Gundlach, L. Margulies, X. Huang, D. J. Jensen (2004): Watching the Growth of Bulk Grains During Recrystallization of Deformed Metals. *Science* **305**(5681): 229-232.

Schwartz, A. J., M. Kumar, B. L. Adams (2000): *Electron backscatter diffraction in materials science*. New York, Kluwer Academic.

Seidman, D. N. (2007): Three-Dimensional Atom-Probe Tomography: Advances and Applications. *Annual Review of Materials Research* **37**(1): 127-158.

Simmons, J., B. Bartha, M. De Graef, M. Comer (2008): Development of Bayesian Segmentation Techniques for Automated Segmentation of Titanium Alloy Images. *Microscopy and Microanalysis* **14**(SupplementS2): 602-603.

Singh, H., A. M. Gokhale, S. I. Lieberman, S. Tamirisakandala (2008): Image based computations of lineal path probability distributions for microstructure representation. *Materials Science and Engineering: A* **474**(1-2): 104-111.

Stutzman, P. (2004): Scanning electron microscopy imaging of hydraulic cement microstructure. *Cement and Concrete Composites* **26**(8): 957-966.

Tiley, J., T. Searles, E. Lee, S. Kar, R. Banerjee, J. C. Russ, H. L. Fraser (2004): Quantification of microstructural features in [alpha]/[beta] titanium alloys. *Materials Science and Engineering A* **372**(1-2): 191-198.

Torquato, S. (2002): *Random heterogeneous materials : microstructure and macroscopic properties*. New York, NY, Springer.

Uchic, M. D., M. A. Groeber, D. M. Dimiduk, J. P. Simmons (2006): 3D microstructural characterization of nickel superalloys via serial-sectioning using a dual beam FIB-SEM. **55**(1): 23-28.

Yeong, C. L. Y., S. Torquato (1998): Reconstructing random media. II. Three-dimensional media from two-dimensional cuts. *Physical Review E* **58**(1): 224.

Zeman, J., M. Sejnoha (2007): From random microstructures to representative volume elements. *Modelling and Simulation in Materials Science and Engineering* (4): S325.